OPEN ACCESS Plant Protection, 10 (02) 2026. 181-198 DOI:10.33804/pp.010.02.5980

Check for updates



Available Online at EScience Press
Plant Protection
ISSN: 2617-1287 (Online), 2617-1279 (Print)
http://esciencepress.net/journals/PP

Research Article

Morphophysiological and Phenological Responses of Wheat Genotypes to Zinc Oxide Nanoparticles under Drought Stress

Madeeha Shirani, Sammer Fatima

Department of Botany, University of Gujrat, Gujrat, Pakistan.

ARTICLE INFO

Article history
Received: 22nd November, 2025
Revised: 9th March, 2026
Accepted: 10th March, 2026

Keywords
Drought stress
Wheat
ZnO nanoparticles
Morpho-physiological traits
Grain filling
Terminal drought.

ABSTRACT

Drought during grain filling limits wheat productivity in arid and semi-arid regions. Zinc oxide nanoparticles (ZnO NPs) may enhance stress tolerance by improving plant physiology and water relations. The present study, therefore, characterized ZnO nanoparticles and evaluated their effects on the morphological, physiological, and phenological responses of wheat genotypes under terminal drought stress. Physicochemical characterization confirmed the successful synthesis of ZnO nanoparticles. Dynamic light scattering analysis revealed a mean hydrodynamic particle diameter of approximately 70 nm. UV-Vis spectroscopy exhibited a characteristic absorption peak around 300 nm, and the optical band gap estimated through a Tauc plot was approximately 2.33 eV. Scanning electron microscopy showed agglomerated clusters of irregular plate- or flake-like nanoparticles with rough surfaces, typical of plant-mediated nanoparticle synthesis. Morphological evaluation indicated that structural traits such as root length, culm length, spike length, and plant height remained relatively stable across treatments, whereas biomass-related traits responded strongly to ZnO application. ZnO nanopriming improved fresh and dry biomass and partially alleviated drought-induced reductions in plant growth. Physiological analyses showed that moderate ZnO treatments enhanced photosynthetic activity, improved relative water content, and increased membrane stability, thereby mitigating the adverse effects of drought stress. Phenological observations further demonstrated that ZnO treatments increased the proportion of the crop cycle devoted to grain filling, particularly under drought conditions. Overall, ZnO nanoparticles improved physiological resilience and grain-filling dynamics under terminal drought. The genotypes MS-14-14C-172 and MS-16-14C-143 exhibited superior performance, highlighting their potential for ZnO-mediated drought management strategies in wheat production systems.

Corresponding Author: Sammer Fatima
Email: sammerfatima339@gmail.com

Introduction

More than half of the world's food supply and a substantial proportion of industrial raw materials are derived from cereals and other crop plants (Benjamin et al., 2025). Major grain crops such as wheat and rice are highly sensitive to water scarcity and exhibit pronounced alterations in morphological and physiological traits under drought conditions (Paul et al., 2019). Water deficit disrupts essential biochemical and physiological processes during both vegetative and reproductive stages,

making drought one of the most critical constraints limiting crop growth and productivity (Fahad et al., 2017). With the global population projected to exceed 9-10 billion by the middle of this century, the increasing frequency and intensity of drought and other abiotic stresses are expected to further exacerbate global food insecurity (Liaqat et al., 2024).

Wheat (*Triticum aestivum* L.) accounts for approximately one-fourth of the global food supply (Vilček and Torma, 2016; Krishnappa et al., 2022). It is nutritionally significant, providing a major portion of global carbohydrate intake as well as a considerable share of dietary protein and energy (Shewry, 2009). In addition, wheat is considered an important cash crop because of its nutritional value, nitrogen content, and broad agronomic importance (Mahajan et al., 2008; Chondie, 2015; Arzani and Ashraf, 2017; Singh et al., 2023a). However, wheat productivity is highly vulnerable to environmental stresses such as heat, drought, and climatic variability, which significantly reduce yield potential (Shiferaw et al., 2013).

Enhancing drought tolerance is therefore essential for stabilizing wheat productivity. Drought is a major factor responsible for reduced crop yields in arid and semi-arid regions (Sharma et al., 2015), and Pakistan's predominantly arid to semi-arid climate makes water scarcity a persistent challenge for wheat production. Yield losses become particularly severe when drought stress coincides with sensitive developmental stages such as tillering and anthesis (Khan et al., 2019). Zinc is an essential micronutrient that plays a vital role in plant growth, development, and stress responses (Gupta et al., 2021; Singh et al., 2023b). Zinc deficiency is associated with impaired stomatal regulation, reduced photosynthetic efficiency, and increased susceptibility to oxidative damage, particularly under drought conditions (Szerement et al., 2022).

In recent years, nanotechnology has emerged as a promising and precision-oriented approach for improving crop productivity and stress resilience (Balusamy et al., 2023; Czarnek et al., 2023; Valle-García et al., 2023). Nanomaterials, typically ranging from 1 to 100 nm in size, often exhibit dose-dependent effects, stimulating plant growth at low concentrations while causing inhibitory effects at higher levels. Among these, zinc oxide nanoparticles (ZnO NPs) have gained considerable attention due to their potential to enhance plant growth and stress tolerance under various abiotic stresses, including drought (El-Saadony et al., 2022; Fatima et al., 2023). ZnO nanoparticles are semiconducting materials with notable UV-Vis optical properties (Jasrotia et al., 2018) and have been reported to improve the morpho-physiological performance of wheat under drought conditions (Kansotia et al., 2024). Previous studies have documented improvements in root and shoot growth, photosynthetic pigments, soluble protein content, relative water content, osmolyte accumulation, and antioxidant enzyme activities following ZnO nanoparticle application (Melash et al., 2023; Raza et al., 2023; Ullah et al., 2023). In addition, increases in chlorophyll *a* and total soluble protein content (Sadati et al., 2022) and enhanced activities of antioxidant enzymes such as superoxide dismutase (SOD) and peroxidase (POD), which mitigate oxidative stress, have been reported (El-Sharkawy et al., 2022). However, excessive application of ZnO nanoparticles may lead to reduced chlorophyll content and increased oxidative stress, highlighting the importance of optimizing application rates (Fatima et al., 2023). Further research is therefore required to determine the most effective and environmentally safe use of ZnO nanoparticles for drought mitigation (Raza et al., 2023).

Accordingly, the present study investigated whether seed priming with ZnO nanoparticles (nanopriming) could mitigate terminal drought stress in bread wheat under pot conditions and assist in identifying drought-tolerant lines with improved growth, physiological performance, and yield. Five lines selected from an initial screening of twenty genotypes were subjected to six ZnO nanopriming-drought treatment combinations. Terminal drought stress was imposed at the grain-filling stage, and morpho-physiological, biochemical, and phenological traits were recorded to elucidate the effects of ZnO nanopriming on plant water relations, membrane stability, photosynthetic performance, and grain development.

The objectives of the study were: (1) to determine the most effective ZnO nanoparticle treatment for alleviating terminal drought stress during the grain-filling stage in wheat; (2) to quantify the changes in morpho-physiological and biochemical traits of wheat lines in response to ZnO nanoparticles under well-watered and drought conditions; and (3) to classify the tested wheat lines according to their drought tolerance based on integrated morphological, physiological, and phenological responses.

Material and Methods

Experiment 1: Germination screening assay

Twenty wheat lines were obtained from BARI (Chakwal) and assigned internal identifiers (MS-1 to MS-20) for tracking throughout the study. A germination percentage test was conducted to select ten healthy wheat lines for subsequent experiments. The germination test for the twenty wheat lines was performed following a standard procedure. Seeds were surface sterilized with 70% ethanol for 2 min, followed by immersion in a 1.5% (w/v) sodium hypochlorite solution for 15 min.

All glassware used during the germination test was thoroughly washed with distilled water, autoclaved, and dried in a hot-air oven before use as shown in Figure 1. After sterilization, the seeds were rinsed three times with sterile distilled water and placed on Petri plates for germination. Germination was monitored for one week, and the germination percentage was calculated accordingly.

Based on a 100% germination rate, ten wheat lines were selected for further experiments. The selected lines were: MS-1 (14C 67), MS-7 (15C 165), MS-8 (13C 084), MS-9 (CH 50), MS-12 (15C 090), MS-13 (17C 210), MS-14 (14C 172), MS-15 (17C 139), MS-16 (14C 143), and MS-20 (15C 110).

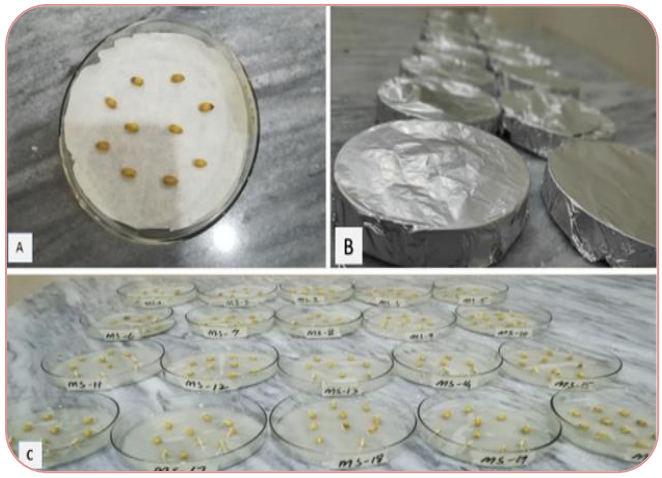


Figure 1. Germination percentage test. The figure illustrates the germination test conducted for the subsequent experiment: (A) arrangement of seeds in a Petri plate for germination; (B) Petri plate covered with aluminum foil; and (C) seed germination observed after 72 h.

Pot experiment

Ten shortlisted wheat lines were evaluated in a preliminary pot screening to identify genotypes with enhanced survival under terminal drought as illustrated in Figure 2. The experiment was conducted with three replicates and continued until the yield stage. Ten seeds were sown per pot (totaling 40 seeds per variety). Two treatments were applied: T0 (well-watered control) and T1 (drought stress, with water withheld at the grain-filling stage). Based on survival rates, five wheat lines were selected for further experiments: MS-1 (14C 67), MS-13 (17C 210), MS-14 (14C 172), MS-15 (17C 139), and MS-16 (14C 143).



Figure 2. Pot experiment on wheat under control and drought stress conditions. (A) arrangement of pots in the experiment; (B) wheat plants at the vegetative stage; (C) reproductive stage of wheat; (D) crop after harvest; and (E) grain yield obtained from the experiment.

Repeat of pot experiment

A pot experiment was conducted in the Botanical Garden, Department of Botany, University of Gujrat, Pakistan, to evaluate the effects of ZnO nanoparticles on five wheat lines under drought stress as shown in Figure 3. The experiment included six treatments with three replicates each. ZnO nanoparticle treatments were applied via seed priming (nanopriming) prior to sowing: seeds were soaked for 20 h in ZnO NP suspensions at concentrations of 10 ppm or 20 ppm, air-dried to surface dryness, and then sown. Terminal drought stress was imposed at the grain-filling stage by withholding irrigation. The treatments were as follows: T0 = well-watered control; T1 = terminal drought (water withheld at grain filling); T2 = 10 ppm ZnO nanopriming (well-watered); T3 = 20 ppm ZnO nanopriming (well-watered); T4 = 10 ppm ZnO nanopriming + terminal drought; T5 = 20 ppm ZnO nanopriming + terminal drought. Morpho-physiological and yield parameters were recorded following the same procedures as in the previous experiment as shown in Figure 4.

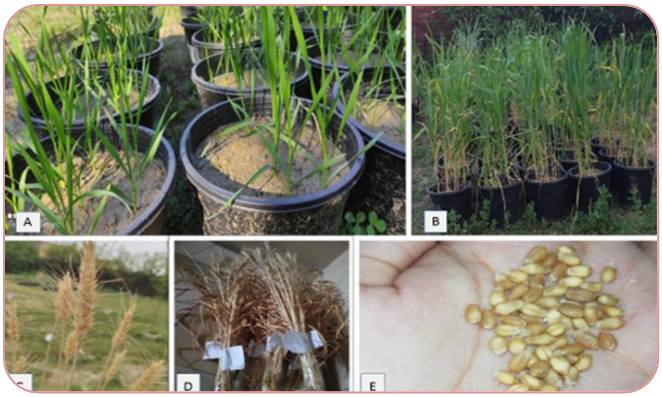


Figure 3. Pot experiment of five wheat lines subjected to six treatments at different growth stages: (A) vegetative stage, (B) reproductive stage, (C) grain-filling stage, (D) post-harvest stage, and (E) yield assessment.

Synthesis of ZnO nanoparticles (green route)

Zinc oxide nanoparticles (ZnO NPs) were synthesized via a green route using *Azadirachta indica* leaf extract as a reducing and capping agent. The leaf extract was prepared by heating the plant material in distilled water, followed by filtration. For nanoparticle synthesis, aqueous solutions of zinc acetate dihydrate and NaOH were prepared separately, mixed under constant stirring, and the leaf extract was added dropwise until a white precipitate formed. The precipitate was collected by filtration, dried at 80°C for 4 h, ground into a fine powder, and calcined at 250°C for 4 h to obtain ZnO nanoparticles.

Morpho-physiological parameters

Maximum root length

The longest root of each plant was measured using a ruler, and root length was recorded in millimeters.

Spike length (cm)

Spike length was measured from the base to the tip, excluding awns, on the mother shoot using a ruler. The average spike length was calculated from three randomly selected spikes per genotype.

Fresh weight of root (g)

Plants were carefully uprooted, and roots were washed thoroughly to remove soil particles. The fresh weight of roots was measured in grams.

Dry weight of root (g)

Freshly harvested roots were oven-dried at 70°C for three days. The dry weight of roots was measured in grams.

Fresh weight of shoot (g)

After 60 days of growth, aboveground plant parts were harvested, and the fresh weight of shoots was measured in grams.

Dry weight of shoot (g)

Detached shoots were oven-dried at 70°C until all moisture was removed, and the dry weight was recorded in grams.

Root-to-shoot ratio (R:S)

The root-to-shoot ratio was calculated as the ratio of root biomass to shoot biomass, indicating the allocation of resources between belowground and aboveground plant parts.

Thousand grain weight (g)

Grains from each genotype were counted to a total of 1,000 and weighed using an electronic balance.

Number of grains per spike

The number of grains per spike was determined by manually counting grains from the mother shoots. The total number of grains per plant was divided by the number of spikes to obtain an average value per spike.

Grain yield (kg ha^{-1})

Grain yield was measured by manually threshing spikes from three randomly selected plants per replicate and weighing the grains using an electronic balance.

Biological yield (kg ha^{-1})

Biological yield was determined as the total oven-dry aboveground biomass (straw + spikes) per replicate.

Harvest index (HI)

Biological yield was determined by randomly selecting plants from each replication of every genotype. The entire plant, including leaves and straw, was harvested and dried, and the total dry biomass was recorded in grams. After threshing the spikes, grain yield per plant was measured by weighing the grains (g). The harvest index (HI) was calculated using the following formula:

$$\mathrm{HI} = \frac{\text{Grain yield}}{\text{Biological yield}} \times 100$$

Data on drought-related and physiological traits associated with crop productivity were collected, and the germplasm was evaluated to determine its level of drought tolerance.

Relative leaf water content (RLWC)

Harvested leaves were immediately placed in test tubes kept on ice to minimize further water loss before determining their fresh weight (FW). For rehydration, 1 ml of distilled water was added to each tube, and the samples were stored at 4°C for 24 h to obtain full turgidity. After rehydration, the leaves were weighed again to record their turgid weight (TW). Subsequently, the leaves were oven-dried at 65°C for 24 h to determine their dry weight (DW).

Relative leaf water content was calculated using the

following formula:

$$\text{RLWC } \% = \frac{\text{FW} - \text{DW}}{\text{TW} - \text{DW}} \times 100$$

Rate of water loss (RWL)

Water loss from excised leaves was determined for each genotype. Fully expanded leaves from the upper canopy were collected and weighed immediately to obtain the initial fresh mass. The leaves were then incubated at 25°C in darkness. After 24 h, the samples were reweighed to determine their mass after water loss. The leaves were subsequently oven-dried at 70°C until a constant mass was obtained, and the dry mass was recorded. The rate of water loss was calculated as:

$$\text{RWL} = \frac{\text{Initial fresh mass } - \text{Mass after 24 h}}{\text{Initial fresh mass}} \times 100$$

Efficiency of water use

Plants were grown in a controlled environment within a growth chamber under a 16/8 h photoperiod, with regulated temperature and humidity conditions. Seeds were germinated at room temperature in uniform small pots. Each pot was covered with a plastic sheet with a small central aperture. The total weight of each pot was recorded, and three additional control pots without plants were used to estimate water loss due to evaporation through the aperture. Plants were grown under conditions where no additional water was available for extraction. Shoots were harvested and weighed to determine their fresh weight. Water use efficiency (WUE) was calculated using the following formula:

Water use by plants = Total weight of each pot once all plant-extractable water has been drained - weight of each pot + fresh shoot and harvested shoot weight – (loss of water in control pots with no plant × 0.7*).

Stability of cell membranes (CMS)

Fresh wheat leaf material was collected from drought-stressed and well-watered control seedlings to assess cell membrane stability (CMS). Leaf surfaces were rinsed with distilled water to remove impurities. Fresh leaf samples were placed in 20 ml flasks and incubated at 25°C for 24 h. Plant material in the flasks was then autoclaved at 121°C for 15 min to release ions. After cooling, the electrical conductivity of the solution was measured using a conductivity meter.

CMS was calculated according to the formula described by Rehman et al. (2016). Two measurements were performed per sample. Leaf samples from control plants were designated as C1 (before electrical injury) and T1 (after electrical injury), while samples from drought-stressed plants were designated as C2 (before electrical injury) and T2 (after electrical injury). Subscripts (1) and (2) were used to distinguish measurements taken before and after autoclaving, respectively.

Chlorophyll analysis

For chlorophyll determination, 10 ml of 80% ethanol was added to test tubes. Fresh leaf samples were cut, weighed, and immediately placed in ethanol (80%) and wrapped to prevent light exposure. The test tubes containing the plant material were incubated in a hot water bath at 80°C for 10 min and then allowed to cool in the dark. Absorbance was measured using a spectrophotometer at 666 nm (Wakeham, 2013).

Root and shoot traits

An efficiently developed root system is critical for optimal water absorption. Crops possess two types of fibrous roots: nodal and seminal roots. Extensive root development can confer advantages under drought conditions. Root morphology significantly influences water and nutrient uptake, and plants with smaller root diameters and greater root lengths typically perform better under arid conditions.

Total protein content

Total protein content was determined following the standard method described by Waterborg (2009). Briefly, 0.1 ml of protein extract was mixed with 5 ml of alkaline copper solution, followed by 0.5 ml of Folin-Ciocalteu reagent. After incubation for 30 min at room temperature in the dark, absorbance was measured at 660 nm using a UV spectrophotometer, with a protein-free solution as the blank. Protein concentration was calculated using a standard curve derived from known protein standards. DNA content and the DNA/protein ratio were also measured as exploratory indicators of cellular integrity under terminal drought and interpreted with caution.

Determination of proline content

Proline content was measured according to Rao et al. (2013). Fresh plant tissue was homogenized in 3% aqueous sulfosalicylic acid at 10,000 rpm. The supernatant was collected for analysis. The assay mixture comprised 2 ml of supernatant, 2 ml of ninhydrin reagent, and 2 ml of glacial acetic acid, which was boiled at 100°C for 1 h. The reaction was terminated immediately by immersing the tubes in ice water. Subsequently, 4 ml of toluene was added to each tube, and absorbance was recorded at 520 nm.

Statistical analysis

The experiment followed a factorial arrangement of genotype × treatment in a completely randomized design with three replicate pots per genotype × treatment combination. Data were analyzed using two-way ANOVA with genotype, treatment, and their interaction as fixed effects (α = 0.05). Model assumptions were assessed using residual diagnostics (normal Q-Q plots and residuals vs. fitted values). When ANOVA revealed significant effects, mean separation was performed using Tukey's HSD test (α = 0.05). To report biological relevance, partial eta-squared (ηp^2) effect sizes were calculated for genotype, treatment, and their interaction. To account for multiple testing across traits, P-values were adjusted within trait families using the Benjamini-Hochberg false discovery rate (FDR) method. All analyses were performed using R and Microsoft Excel. Results are reported as mean ± SD.

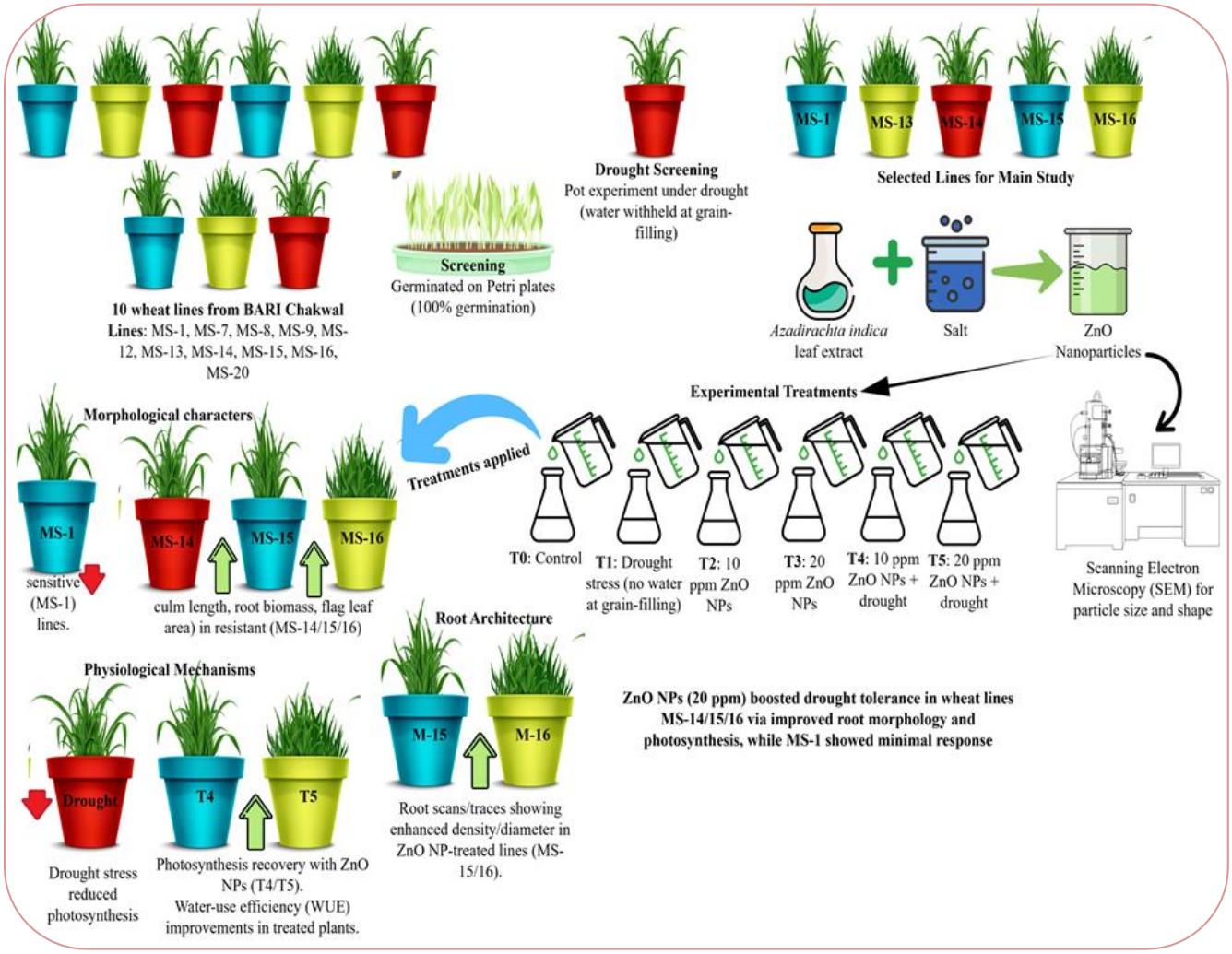


Figure 4. Flow diagram of the experimental methodology.

Results

Physicochemical characterization of ZnO nanoparticles

The particle size distribution of ZnO nanoparticles (ZnO NPs) in aqueous suspension was determined using dynamic light scattering (DLS) with a particle size analyzer. For the analysis, ZnO NPs were dispersed in deionized water to obtain a homogeneous suspension and transferred into a cuvette for measurement. The mean hydrodynamic diameter of the nanoparticles was approximately 70 nm (Figure 5A).

Ultraviolet-visible (UV-Vis) absorbance spectra were recorded in the range of 250-800 nm to confirm the optical characteristics of ZnO NPs. A distinct absorption peak at approximately 300 nm was observed (Figure

5B), which is consistent with previous reports on biosynthesized ZnO nanoparticles. The optical band gap was estimated using a Tauc plot and was determined to be approximately 2.33 eV (Figure 5C).

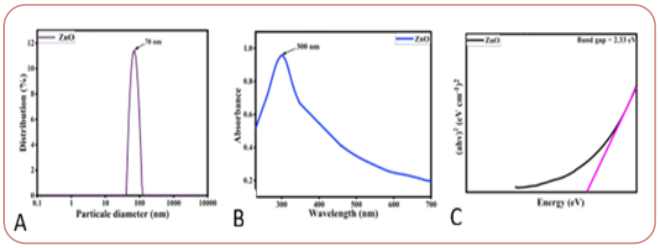


Figure 5. Physicochemical characterization of green-synthesized ZnO nanoparticles. (A) Dynamic light scattering (DLS) particle size distribution showing a mean hydrodynamic diameter of approximately 70 nm. (B) UV-Vis absorption spectrum (250-800 nm) exhibiting a characteristic absorption peak near 300 nm. (C) Tauc plot used to estimate the optical band gap (~2.33 eV) of the ZnO nanoparticles.

The morphology of the nanoparticles was examined using scanning electron microscopy (SEM). SEM micrographs obtained at different magnifications revealed agglomerated nanoparticle clusters composed of irregular plate- or flake-like crystallites with rough surfaces (Figure 6). Such morphology is commonly reported for plant-mediated ZnO nanoparticle synthesis due to biomolecule-driven capping and aggregation.

Morphological analysis

The structural length traits remained relatively stable across the five treatments (T1-T5) used for morphological evaluation. Root length, culm length, spike length, and plant height exhibited only minor variations among treatments and genotypes, with no evidence of pronounced dwarfing or excessive elongation under any ZnO nanoparticle application or drought regime (Figure 7A-D). These observations indicate that the imposed treatments primarily influenced biomass accumulation rather than overall plant architecture.

In contrast, biomass-related traits were clearly responsive to the treatments. Fresh and dry weights of the culm, spikes, roots, and whole plants exhibited wide variation among genotype × treatment combinations and effectively distinguished vigorous entries from weaker ones (Figure 8). ZnO nanopriming under non-drought conditions, as well as its combination with drought stress, generally supported higher shoot and spike biomass compared with drought stress alone. In several genotypes, ZnO application partially mitigated the reductions in biomass caused by water withholding. However, the combined treatment of ZnO and drought did not fully restore growth to the levels observed under the best non-stress conditions, and the highest biomass values were typically recorded when ZnO was applied under well-watered or only moderately stressed conditions.

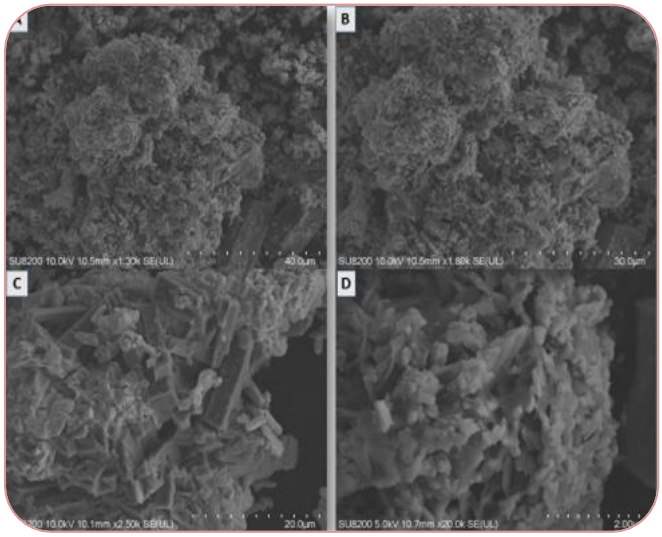


Figure 6. SEM morphology of green-synthesized ZnO nanoparticles. Scanning electron microscopy (SEM) micrographs at increasing magnifications show agglomerated clusters of ZnO nanoparticles. (A-B) Low-magnification images highlight porous, clustered aggregates, whereas (C-D) higher-magnification images reveal irregular plate- or flake-like crystallites with rough surfaces forming larger agglomerates (scale bars as indicated).

When traits were averaged across treatments, clear genotypic differences became evident. MS-14-14C-172 and MS-16-14C-143 consistently produced higher fresh and dry plant biomass as well as greater spike-related weights than the other lines, identifying them as the most vigorous genotypes in terms of structural growth and reproductive biomass. MS-13-17C-210 and MS-15-17C-139 generally exhibited intermediate performance, whereas MS-1-14C-67 frequently showed lower whole-plant biomass, indicating greater sensitivity to stress or lower inherent vigor. Differences among genotypes in root, culm, and plant length were relatively small, supporting the view that total biomass production, rather than plant stature, primarily distinguishes the genotypes.

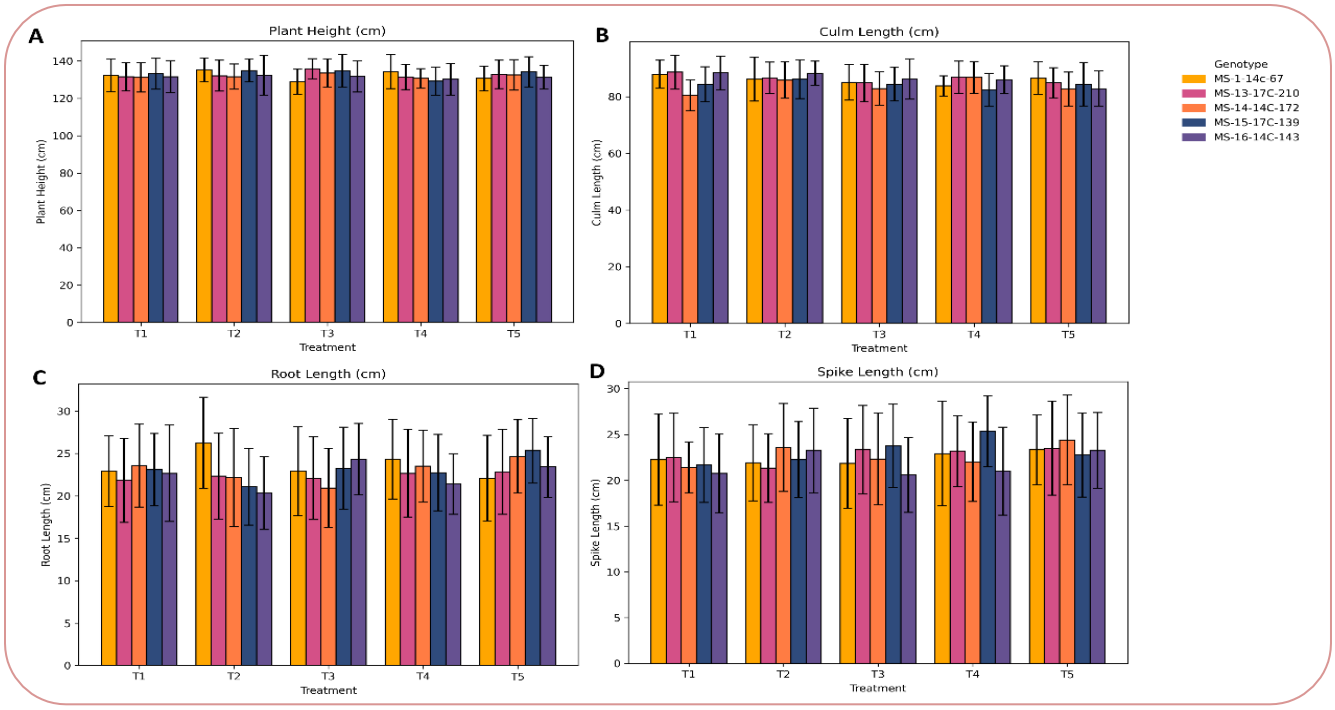


Figure 7. Structural morphological traits of wheat genotypes under different treatments. Bar graphs showing plant height (A), culm length (B), root length (C), and spike length (D) (cm) of five wheat genotypes under five treatments (T1–T5). Each genotype is represented by a different color: MS-1-14C-67 (orange), MS-13-17C-210 (red), MS-14-14C-172 (pink), MS-15-17C-139 (blue), and MS-16-14C-143 (purple). Error bars represent standard deviation (SD). The results illustrate the variation in structural morphological traits among genotypes across different treatments.

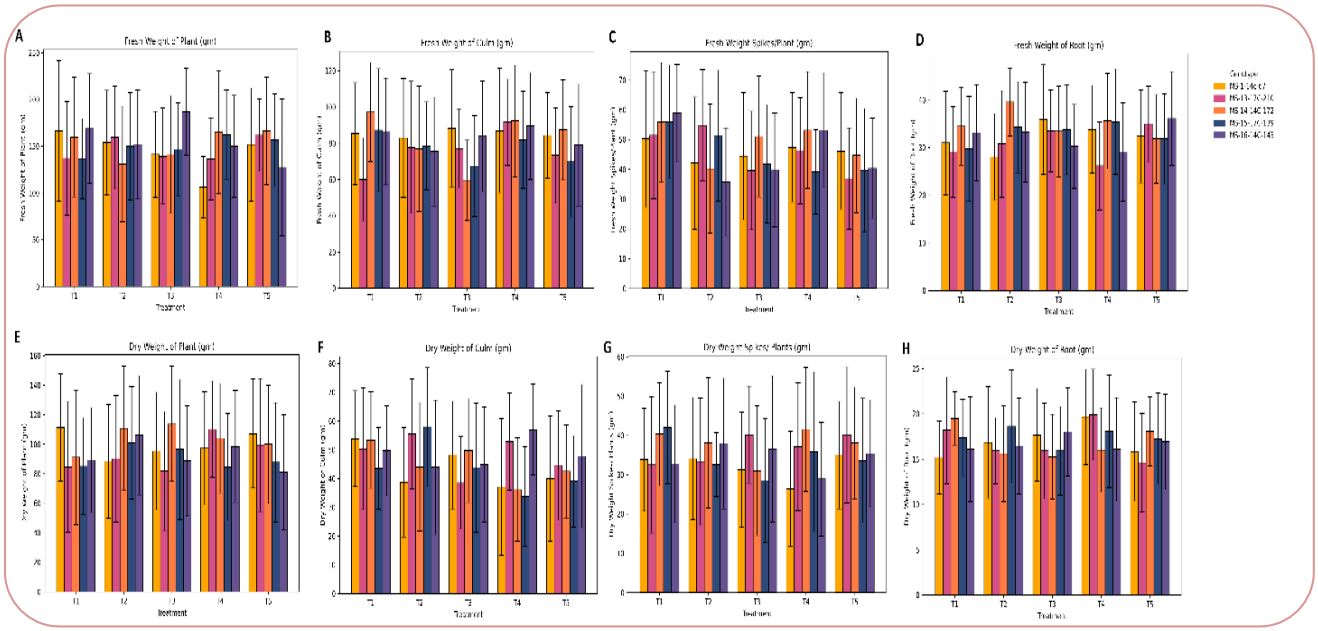


Figure 8. Biomass response of wheat genotypes to different treatments. Bar graphs showing the fresh and dry biomass (g) of different plant parts, including fresh weight of plant (A), fresh weight of culm (B), fresh weight of spikes per plant (C), fresh weight of root (D), dry weight of plant (E), dry weight of culm (F), dry weight of spikes per plant (G), and dry weight of root (H), in five wheat genotypes under five treatments (T1–T5). Error bars represent the standard deviation of the mean. The data illustrate the patterns of biomass accumulation in response to the applied treatments.

Trait association analysis

Relationships among traits were examined using Pearson correlation matrices calculated from genotype × treatment means to visualize co-variation among biomass, physiological, and morphological traits. Because these correlations are descriptive and based on treatment means, they were used to support the interpretation of ANOVA results rather than as independent hypothesis tests. In the present dataset, biomass-related traits clustered together and showed strong positive associations, whereas length-related traits exhibited comparatively weaker correlations with biomass (Figures 9 and 10).

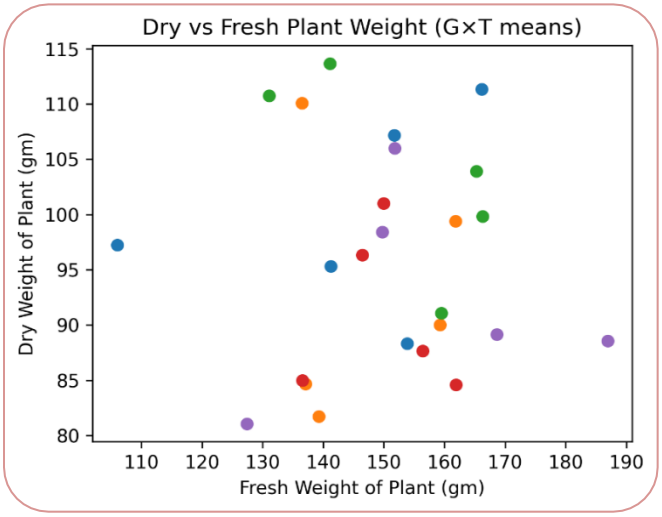


Figure 9. Correlation between fresh and dry plant weights. Scatter plot illustrating the relationship between fresh and dry plant weights (g) of wheat genotypes based on genotype × treatment (G × T) means. The figure highlights the association between fresh and dry biomass across different treatments.

Physiological and biochemical responses

The physiological traits of wheat genotypes exhibited clear, treatment-dependent responses to drought stress and ZnO nanoparticle application. Across all genotypes, drought stress alone (T1) resulted in a slight reduction in the net photosynthetic rate compared with the well-watered control (T0). In contrast, ZnO nanopriming treatments (T2 and particularly T3) enhanced photosynthetic activity beyond the control level, with T3 producing the highest mean assimilation rate.

Under the combined ZnO and drought treatments (T4 and T5), photosynthetic activity partially recovered relative to T1, indicating that ZnO nanoparticles mitigated some of the adverse effects of terminal drought stress.

Transpiration followed a similar trend, reaching its maximum at intermediate ZnO levels and declining under higher stress intensity. Water-use efficiency tended to decrease in treatments with the highest assimilation rates but improved slightly in treatments where photosynthesis and transpiration were more balanced in Figure 11.

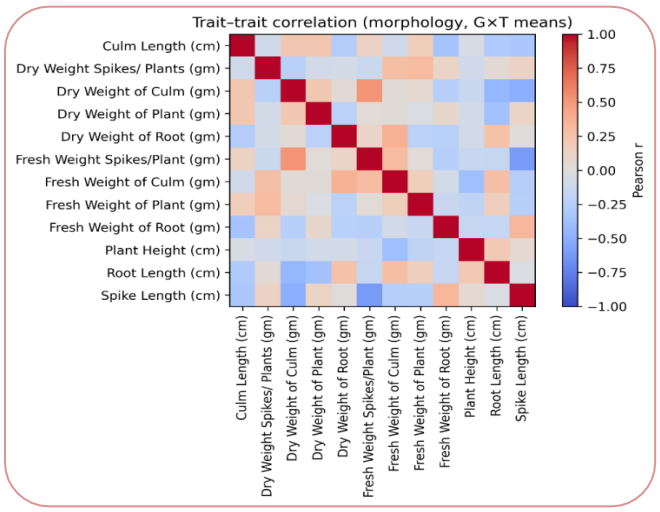


Figure 10. Trait-trait correlation matrix of wheat genotypes across treatments. Heatmap illustrating Pearson correlation coefficients among morphological traits (cm and g) of wheat genotypes based on genotype × treatment (G×T) mean values.

Water status and membrane integrity were more sensitive to drought stress than gas exchange parameters. RWC declined from the control level to its lowest values under drought treatment alone (T1), confirming that terminal drought significantly reduced leaf hydration. ZnO nanoparticle treatments at T2 and T4 restored RWC to levels comparable to, or slightly higher than, the control, whereas T3 and T5 showed partial recovery.

A similar trend was observed for membrane stability. Membrane stability was markedly reduced under T1 but reached the highest mean values at T3, while T2 and T4 also exhibited improved stability compared with the control. These findings suggest that ZnO nanoparticles, particularly at moderate concentrations, contributed to the protection of cellular membranes and helped maintain tissue water status under drought stress.

Leaf osmotic potential became slightly more negative with increasing treatment levels, indicating a modest osmotic adjustment in response to increasing stress intensity.

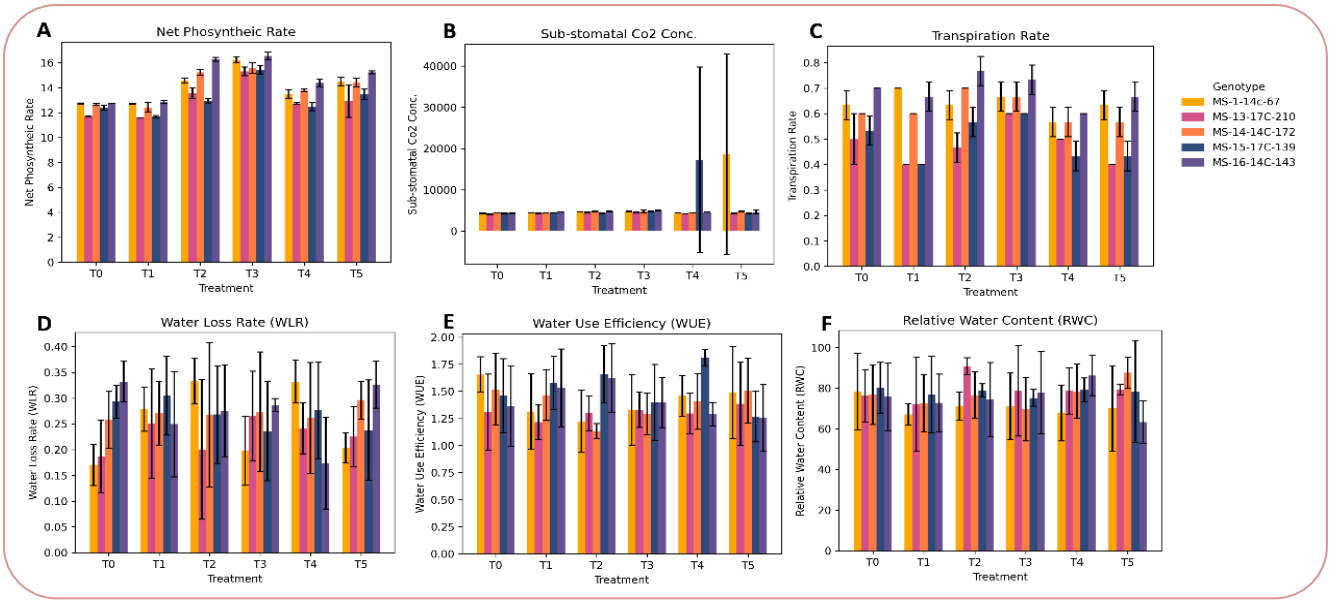


Figure 11. Physiological and biochemical responses of five wheat genotypes to six treatments (T0-T5). Bar graphs depicting: (A) net photosynthetic rate, (B) sub-stomatal CO_2 concentration, (C) transpiration rate, (D) water loss rate, (E) water use efficiency, and (F) relative water content (RWC) across five wheat genotypes under six treatment conditions.

Chlorophyll fractions (Chl a, Chl b, and Chl c) exhibited a gradual decline from T0 to T5, indicating progressive pigment loss with increasing treatment intensity as shown in Figure 12. In contrast, the composite chlorophyll index decreased under drought alone but subsequently increased, reaching a maximum at T3, which coincided with the highest photosynthetic rate and membrane stability. This close association among chlorophyll status, gas exchange, and membrane integrity suggests that ZnO nanoparticles (ZnO NPs), when applied at optimal levels, helped preserve the functionality of the photosynthetic apparatus under terminal drought conditions.

Osmolytes and soluble reserves exhibited a stage-dependent response under terminal drought stress. The concentrations of proline, total soluble sugars, and total soluble proteins did not increase in the overall treatment means; instead, they showed a slight decline from the control toward the most severe stress combinations as shown in Figure 12. Under drought imposed during the grain-filling stage, osmolyte pools may increase transiently during the early phase of stress but subsequently decline due to remobilization to developing sinks and accelerated senescence under prolonged water deficit as shown in Figure 13. In this context, the relatively lower proline levels observed under ZnO nanopriming treatments may also indicate partial stress alleviation (i.e., reduced stress signaling), particularly when accompanied by improved plant water status and enhanced membrane stability. Consequently, DNA content and the DNA/protein ratio should be interpreted cautiously as exploratory indicators that may reflect changes in cellular integrity and tissue turnover under terminal stress rather than serving as primary mechanisms of drought tolerance.

Clear genotypic differences were evident when physiological traits were averaged across treatments as illustrated in heatmap Figure 14. MS-16-14C-143 exhibited the highest net photosynthetic rate and transpiration, favorable water-use efficiency, the most negative osmotic potential, a high chlorophyll index, and superior membrane stability. Collectively, these traits characterize a physiologically tolerant profile under ZnO-mediated drought management. In contrast, MS-1-14C-67 maintained the highest chlorophyll fractions, DNA content, structural proteins, soluble sugars and proteins, and proline levels; however, it displayed comparatively lower RWC and a less negative osmotic potential, suggesting a strategy based on pigment and reserve maintenance rather than strong water-relation regulation. MS-13-17C-210 generally showed weaker gas-exchange capacity and lower membrane stability despite relatively high RWC, indicating comparatively lower physiological efficiency under the tested conditions. The genotypes MS-14-14C-172 and MS-15-17C-139 exhibited intermediate responses between these extremes.

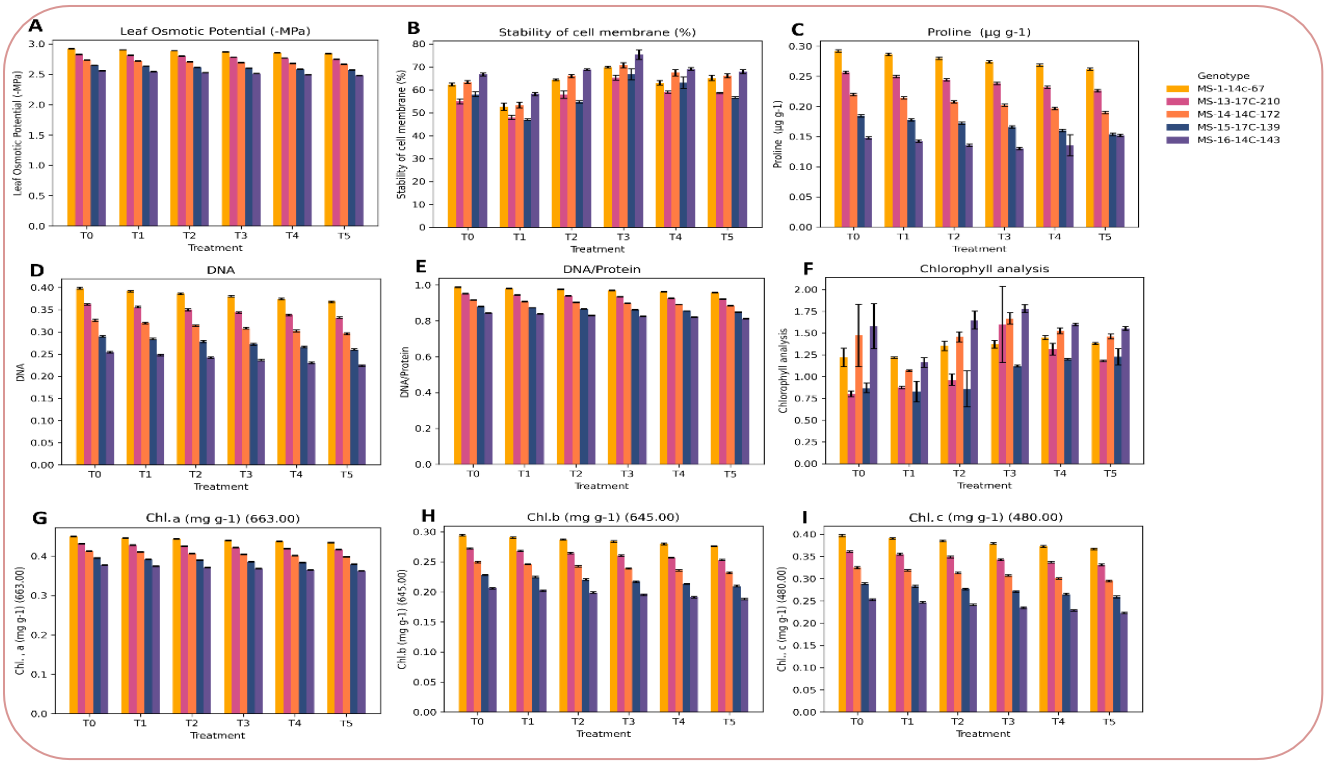


Figure 12. Biochemical and physiological analysis of wheat genotypes. Bar graphs depicting the biochemical and physiological responses of wheat genotypes across six treatments (T0-T5), including leaf osmotic potential (A), membrane stability index (B), proline content (C), DNA content (D), DNA/protein ratio (E), and chlorophyll content (F–I). Chlorophyll a (G), chlorophyll b (H), and chlorophyll c (I) are expressed in mg g^{-1} fresh weight.

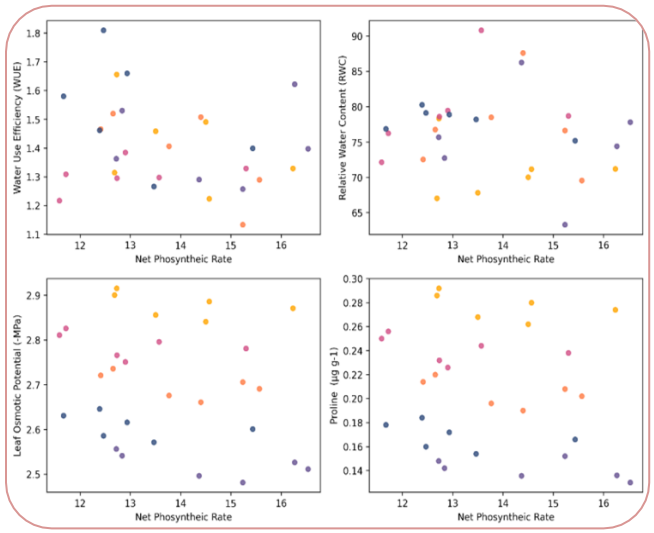


Figure 13. Relationships between net photosynthesis and key water-related and osmolyte traits. Scatter plots illustrating the relationships between net photosynthetic rate (x-axis) and selected water-related and osmolyte traits (y-axis): water use efficiency (A), relative water content (B), leaf osmotic potential (C), and proline content (D).

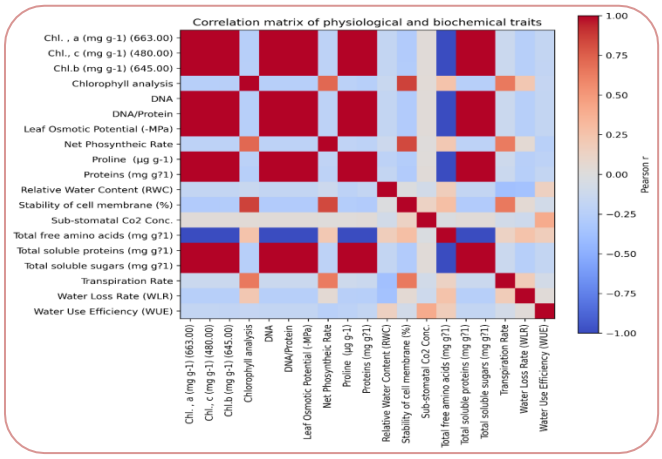


Figure 14. Correlation matrix of physiological and biochemical traits. Heatmap illustrating the Pearson correlation coefficients among key physiological and biochemical traits, including leaf osmotic potential, net photosynthetic rate, proline content, relative water content (RWC), chlorophyll content, DNA, and protein levels. The color scale ranges from dark blue (strong negative correlation) to dark red (strong positive correlation), emphasizing the interrelationships among these traits.

Phenological responses

Phenological traits, expressed as percentages of the crop life cycle, indicated that the overall developmental framework was largely conserved; however, the allocation of time among the pre-anthesis, grain-filling, and post-anthesis phases was sensitive to drought stress and ZnO nanoparticle treatments as shown in Figure 15. Crown root initiation remained nearly constant at approximately 14% across all genotype × treatment combinations, suggesting that the earliest stage of root establishment was not influenced by the applied management strategies. Similarly, phenological parameters such as heading duration, booting-to-maturity, and heading-to-maturity intervals varied only slightly (1-3 percentage points) among treatments and genotypes. This minimal variation indicates that the fundamental structure of the growth cycle remained stable even under terminal drought conditions.

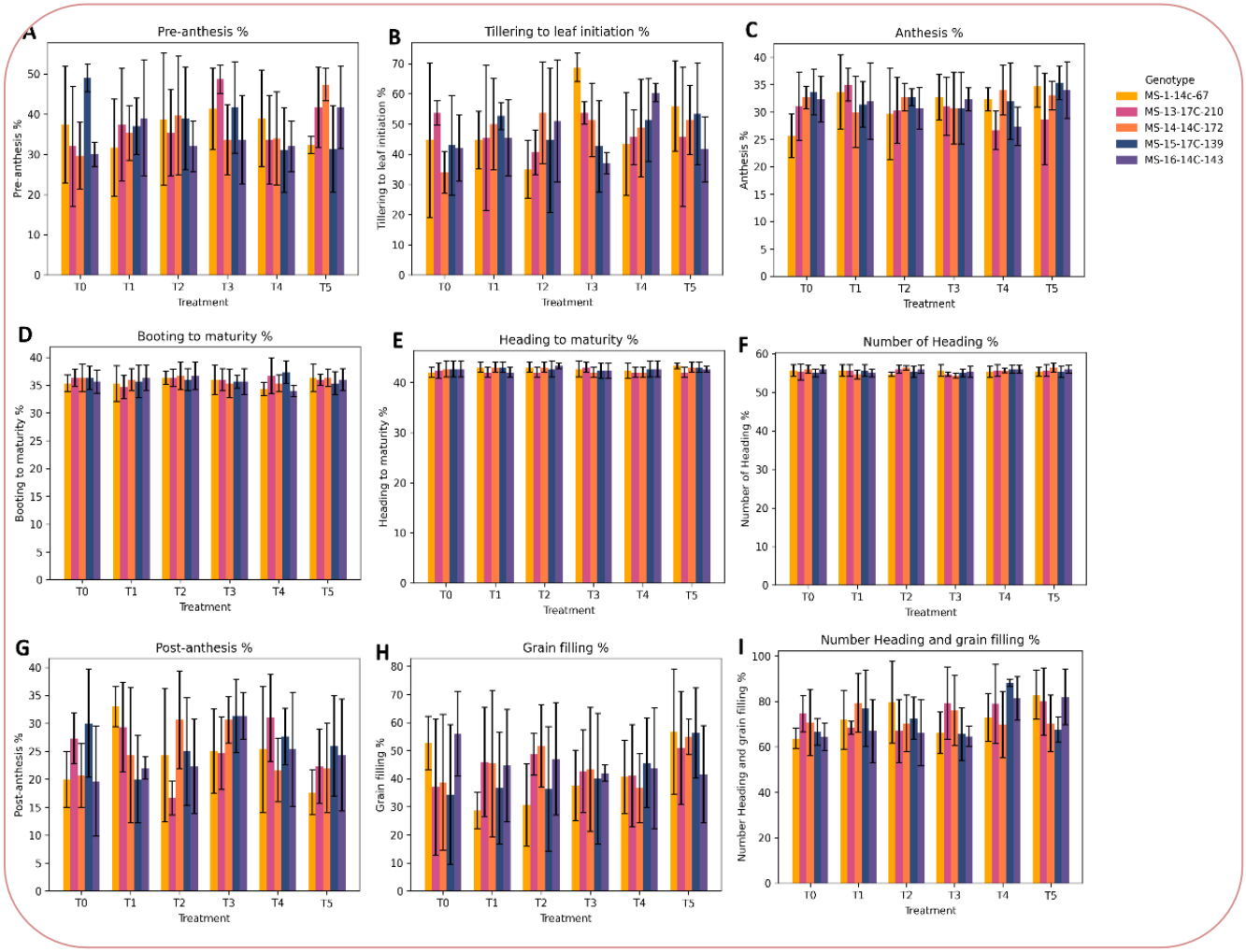


Figure 15. Phenological stage percentages of five wheat genotypes under six treatments (T0-T5). Bar graphs showing the percentage of plants at different phenological stages: pre-anthesis (A), tillering to leaf initiation (B), anthesis (C), booting to maturity (D), heading to maturity (E), number of heading (F), post-anthesis (G), grain filling (H), and combined heading and grain filling (I) across five wheat genotypes subjected to six treatments.

The clearest treatment effects were observed in the tillering-to-leaf initiation phase, the combined heading and grain-filling period, the grain-filling proportion, and the relative balance between pre-anthesis and post-anthesis phases. Drought stress alone (T1) increased the proportion of the crop cycle allocated to the early vegetative stage compared with the control, while reducing the relative duration of the grain-filling phase as shown in Figure 16.

Application of ZnO nanoparticles, either under well-

watered conditions or in combination with drought stress, altered these temporal proportions. Treatments T3, T4, and T5 extended the tillering-to-leaf initiation phase and, more importantly, increased the proportion of the growth cycle occupied by the heading and grain-filling stages, with T4 and T5 exhibiting the highest values for this composite period.

The grain-filling proportion declined under drought alone relative to the control; however, it increased under selected ZnO plus drought treatments. Among these, T5 produced the greatest improvement and even exceeded the grain-filling proportion observed in the control treatment.

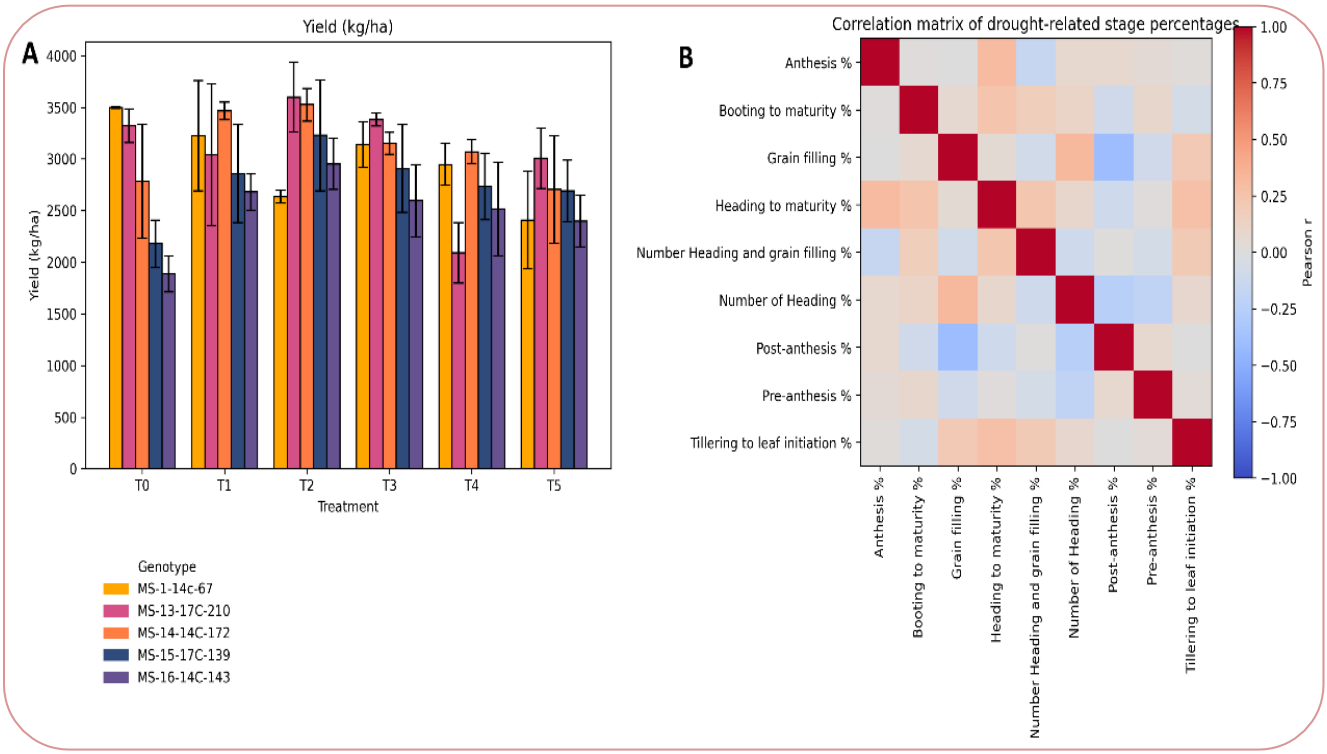


Figure 16. Yield and correlation of drought-related phenological stages. (A) Bar graph depicting grain yield (kg/ha) of five wheat genotypes across six treatments (T0–T5), with each genotype color-coded: MS-1-14C-67 (orange), MS-13-17C-210 (red), MS-14-14C-172 (pink), MS-15-17C-139 (blue), and MS-16-14C-143 (purple). Error bars indicate standard deviation. (B) Pearson correlation matrix showing the relationships between percentages of different drought-related phenological stages.

Phenological dynamics and grain filling

The distribution between the pre-anthesis and post-anthesis periods further supports this pattern. Certain treatments, such as T3, extended both the pre-anthesis and post-anthesis phases, whereas T5 shortened the post-anthesis phase but still resulted in a high grain-filling percentage. This suggests that specific combinations of ZnO nanoparticles and drought stress promoted more efficient grain filling within a relatively shorter late-season period, rather than merely prolonging the entire post-anthesis phase.

Genotype-level averages across treatments showed that MS-14-14C-172 and MS-16-14C-143 maintained the largest grain-filling window on a percentage basis, followed closely by MS-13-17C-210 and MS-15-17C-139, whereas MS-1-14C-67 exhibited the smallest grain-filling percentage. These phenological responses were consistent with the drought-tolerance ranking inferred from morphological and physiological traits, with MS-14-14C-172 and MS-16-14C-143 combining favourable phenological characteristics with stronger physiological performance.

Correlation analysis indicated that grain-filling percentage was moderately negatively associated with the clearly defined post-anthesis duration as shown in Figure 17. Thus, treatments that allocated a greater proportion of the crop cycle to the grain-filling phase tended to achieve improved grain filling, even when the nominal post-anthesis period was comparatively shorter.

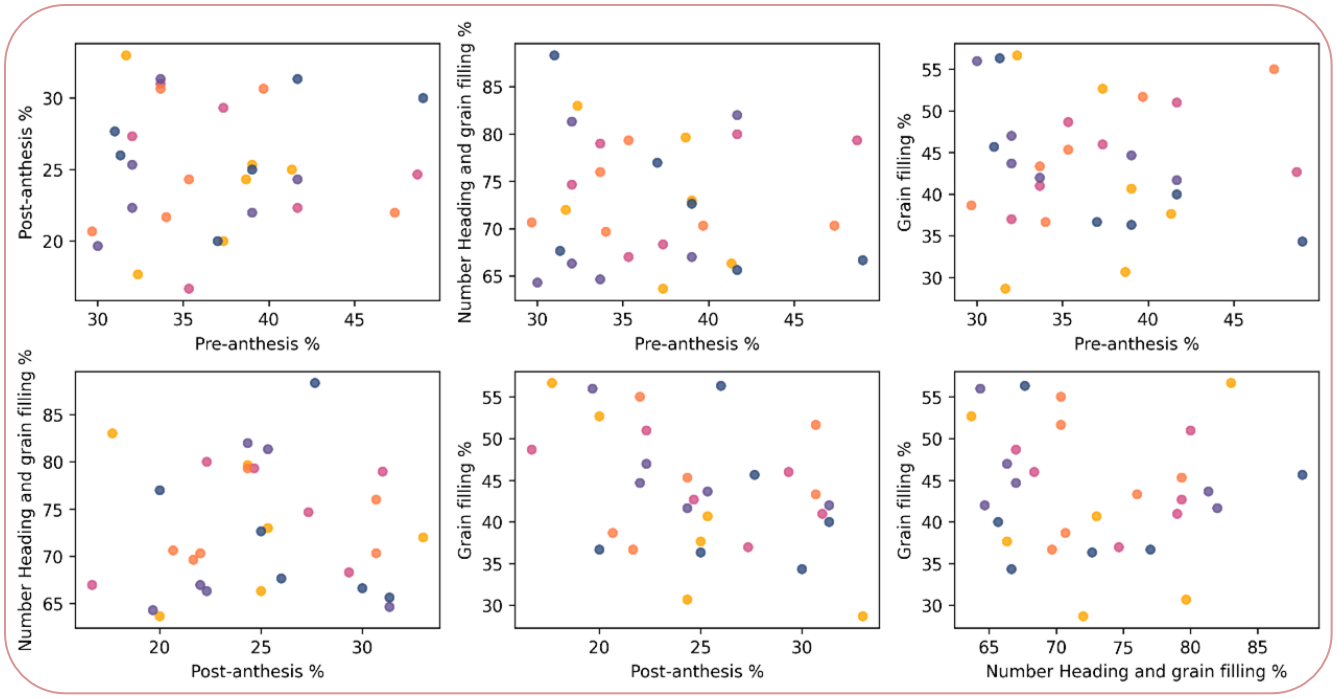


Figure 17. Correlations among key phenological percentages in wheat genotypes. Scatter plots depicting the relationships among major phenological stages, pre-anthesis (%), post-anthesis (%), number of heading and grain filling (%), and grain filling (%), across different treatments. Genotypes are color-coded as follows: MS-1-14C-67 (orange), MS-13-17C-210 (red), MS-14-14C-172 (pink), MS-15-17C-139 (blue), and MS-16-14C-143 (purple).

Discussion

Terminal drought during the grain-filling stage markedly reduced wheat growth and yield in this pot experiment, corroborating previous findings that flowering and grain filling represent some of the most drought-sensitive developmental stages in cereals (Hameed et al., 2011; Farooq et al., 2014). Across the five tested wheat lines, water withholding at the grain-filling stage (T1) significantly reduced shoot and spike biomass, thousand-grain weight, and grain yield compared with the well-watered control. In contrast, structural traits such as plant height, culm length, and spike length were comparatively less affected. This pattern suggests that drought primarily constrained biomass accumulation and assimilate partitioning to the grains rather than altering overall plant stature.

Seed priming with ZnO nanoparticles (nanopriming) modified these responses in a dose-dependent manner. Under non-stress conditions, both 10 and 20 ppm ZnO treatments (T2 and T3) increased shoot and spike biomass relative to the control, while the 10 ppm treatment produced the highest mean grain yield. These results support earlier reports indicating that moderate zinc supplementation can enhance growth and yield in wheat (Melash et al., 2023; Raza et al., 2023). Under drought conditions, the combined ZnO and drought treatments (T4 and T5) improved biomass production and grain yield compared with drought alone; however, they did not fully restore yield to the level achieved under well-watered conditions with ZnO treatment. This finding suggests that ZnO nanoparticles can alleviate, but not completely offset, the detrimental effects of terminal drought, and that genotype × treatment interactions remain critical determinants of performance.

The physiological responses further elucidate the mechanisms underlying this mitigation. Drought stress alone reduced RWC from 80.0% in the control to 72.3% and decreased the membrane stability index (MSI) from 61.1% to 51.9%, indicating impaired tissue hydration and increased membrane damage. ZnO nanopriming, particularly at 20 ppm, increased MSI to approximately 69.6% and maintained higher chlorophyll index and gas exchange rates compared with untreated plants. Under combined stress conditions, ZnO treatments restored RWC toward control levels (approximately 78% for T2 and T4) and partially improved membrane stability.

These observations are consistent with the notion that ZnO nanoparticles enhance water relations, maintain membrane integrity, and support photosynthetic activity under stress conditions (Sadati et al., 2022; Fatima et al., 2023; Kansotia et al., 2024).

Phenological traits expressed as percentages of the crop life cycle indicated that the overall developmental structure remained largely conserved; however, the distribution of time between pre-anthesis and post-anthesis phases was sensitive to both water availability and ZnO treatments. Terminal drought reduced the effective grain-filling duration from 43.7% of the life cycle in the control to 40.3% in T1. In contrast, ZnO combined with drought (particularly T5) increased the grain-filling proportion to 52.1%, exceeding the control. Treatments T3, T4, and T5 also increased the proportion of the crop cycle occupied by the heading and grain-filling stages compared with T0. These findings suggest that ZnO nanopriming helped maintain functional leaves and reproductive structures for a longer period under drought, thereby facilitating more efficient remobilization of assimilates to developing grains during a critical reproductive stage (Pandya et al., 2023).

Genotype-specific responses observed across the morphological, physiological, and phenological datasets revealed contrasting drought adaptation strategies. The lines MS-14-14C-172 and MS-16-14C-143 consistently accumulated greater fresh and dry biomass, maintained higher spike weights, and produced higher grain yield compared with the other lines. These genotypes also maintained favorable RWC, MSI, and grain-filling percentages, indicating both morphological vigor and physiological resilience under ZnO-mediated drought conditions. MS-13-17C-210 and MS-15-17C-139 exhibited intermediate performance, whereas MS-1-14C-67 frequently produced the lowest biomass and grain yield. Nevertheless, this genotype maintained relatively higher levels of pigments, DNA, structural proteins, soluble sugars, total proteins, and proline, despite lower RWC and a less negative osmotic potential. Such responses suggest a drought adaptation strategy based primarily on biochemical adjustment and metabolic reserve accumulation rather than the maintenance of strong water relations and growth (Ullah et al., 2022; Li et al., 2021).

Overall, the combined evidence from morphological, physiological, and phenological traits supports a model in which moderate doses of ZnO nanopriming alleviate terminal drought stress primarily by stabilizing plant water status and membrane integrity, sustaining photosynthetic capacity, and reallocating a greater proportion of the crop life cycle toward grain filling. These beneficial effects were most pronounced in inherently vigorous genotypes such as MS-14-14C-172 and MS-16-14C-143, highlighting the importance of aligning nanoparticle-based interventions with the genetic background of the crop. However, grain yield under drought conditions with ZnO treatment remained lower than that observed under optimal water supply with ZnO, indicating that nanoparticle applications cannot substitute for adequate water management. Therefore, field validation across multiple seasons and environments, involving a broader range of ZnO concentrations and additional genotypes, is necessary before translating these findings into practical recommendations for drought-prone wheat production systems.

Conclusion

The results of this study demonstrate that terminal drought during the grain-filling stage severely restricts wheat productivity by reducing biomass accumulation, plant water status, membrane stability, grain filling, and ultimately grain yield. Seed priming with ZnO nanoparticles at moderate concentrations (10-20 ppm) significantly improved morpho-physiological performance under both well-watered and drought conditions. The 10 ppm treatment produced the highest mean grain yield under non-stress conditions, while both ZnO doses enhanced photosynthetic activity, shoot and spike biomass, and membrane integrity.

Under drought conditions, ZnO treatments partially restored relative water content and membrane stability and helped sustain the grain-filling period, thereby reducing, although not completely eliminating, the yield losses associated with terminal drought stress. Integrated analysis of morphological, physiological, and phenological traits identified MS-14-14C-172 and MS-16-14C-143 as the most promising genotypes for ZnO-mediated drought tolerance, as they consistently maintained higher biomass production, stable RWC and MSI, heavier spikes, and superior grain yield across treatments.

Overall, moderate ZnO nanopriming represents a promising complementary strategy that can be integrated with breeding programs and improved agronomic practices to enhance yield stability in wheat grown under drought-prone environments.

Author Contribution

SF conceived and supervised the study, contributed to the study design, assisted with data interpretation, and critically revised the manuscript. MS performed the experimental work, collected and analyzed the data, and prepared the initial draft of the manuscript. Both authors have read and approved the final version of the manuscript.

Research Funding

This research did not receive any grant from funding agencies.

Conflict of Interest

The authors declare no conflict of interest.

Sustainable Development Goals Targeted

SDG 2: Zero Hunger
SDG 6: Clean Water and Sanitation
SDG 13: Climate Action

Policy Addressed

This study aligns with national climate-smart agriculture and food security policies by promoting drought-tolerant wheat, nano-seed priming, and precision zinc use for sustainable productivity under water stress.

References

Arzani, A., Ashraf, M., 2017. Cultivated ancient wheats (*Triticum* spp.): A potential source of health-beneficial food products. Comprehensive Reviews in Food Science and Food Safety 16(3), 477-488.

Balusamy, S.R., Joshi, A.S., Perumalsamy, H., Mijakovic, I., Singh, P., 2023. Advancing sustainable agriculture: A critical review of smart and eco-friendly nanomaterial applications. Journal of Nanobiotechnology 21(1), 372.

Benjamin, J., Idowu, O., Babalola, O.K., Oziegbe, E.V., Oyedokun, D.O., Raheem, J., Omole, A., Hussayn, A.Q., Akinyemi, A.M., Adebayo, A., 2025. Status of cereal production in Africa: Insights from abiotic stressors in a changing climate-a short review. Discover Agriculture 3(1), 115.

Chondie, Y.G., 2015. Effect of integrated nutrient management on wheat: A review. Journal of Biology, Agriculture and Healthcare 13(5), 68-76.

Czarnek, K., Tatarczak-Michalewska, M., Dreher, P., Rajput, V.D., Wójcik, G., Gierut-Kot, A., Szopa, A., Blicharska, E., 2023. UV-C seed surface sterilization and Fe, Zn, Mg, Cr biofortification of wheat sprouts as an effective strategy of bioelement supplementation. International Journal of Molecular Sciences 24(12), 10367.

El-Saadony, M.T., Saad, A.M., Soliman, S.M., Salem, H.M., Desoky, E.S.M., Babalghith, A.O., El-Tahan, A.M., Ibrahim, O.M., Ebrahim, A.A., Abd El-Mageed, T.A., Elrys, A.S., 2022. Role of nanoparticles in enhancing crop tolerance to abiotic stress: A comprehensive review. Frontiers in Plant Science 13, 946717.

El-Sharkawy, M., Mahmoud, E., Abd El-Aziz, M., Khalifa, T., 2022. Effect of zinc oxide nanoparticles and soil amendments on wheat yield, physiological attributes and soil properties grown in saline–sodic soil. Communications in Soil Science and Plant Analysis 53(17), 2170-2186.

Fahad, S., Bajwa, A.A., Nazir, U., Anjum, S.A., Farooq, A., Zohaib, A., Sadia, S., Nasim, W., Adkins, S., Saud, S., Ihsan, M.Z., 2017. Crop production under drought and heat stress: Plant responses and management options. Frontiers in Plant Science 8, 1147.

Farooq, M., Hussain, M., Siddique, K.H., 2014. Drought stress in wheat during flowering and grain-filling periods. Critical Reviews in Plant Sciences 33(4), 331-349.

Fatima, A., Safdar, N., Ain, N.U., Yasmin, A., Chaudhry, G.E.S., 2023. Abscisic acid-loaded ZnO nanoparticles as drought tolerance inducers in *Zea mays* L. with physiological and biochemical attributes. Journal of Plant Growth Regulation 42(11), 7280-7293.

Gupta, P.K., Balyan, H.S., Sharma, S., Kumar, R., 2021. Biofortification and bioavailability of Zn, Fe and Se in wheat: Present status and future prospects. Theoretical and Applied Genetics 134(1), 1-35.

Jasrotia, P., Kashyap, P.L., Bhardwaj, A.K., Kumar, S., Singh, G.P., 2018. Scope and applications of nanotechnology for wheat production: A review of recent advances. Wheat and Barley Research 10(1), 1-14.

Kansotia, K., Naresh, R., Sharma, Y., Sekhar, M., Sachan, P., Baral, K., Pandey, S.K., 2024. Nanotechnology-driven solutions: Transforming agriculture for a sustainable and productive future. Journal of Scientific Research and Reports 30(3), 32-51.

Khan, Z.S., Rizwan, M., Hafeez, M., Ali, S., Javed, M.R., Adrees, M., 2019. The accumulation of cadmium in wheat (*Triticum aestivum*) as influenced by zinc oxide nanoparticles and soil moisture conditions. Environmental Science and Pollution Research

26(19), 19859-19870.

Krishnappa, G., Khan, H., Krishna, H., Kumar, S., Mishra, C.N., Parkash, O., Devate, N.B., Nepolean, T., Rathan, N.D., Mamrutha, H.M., Srivastava, P., 2022. Genetic dissection of grain iron and zinc, and thousand kernel weight in wheat (*Triticum aestivum* L.) using genome-wide association study. Scientific Reports 12(1), 12444.

Li, Y., Liang, L., Li, W., Ashraf, U., Ma, L., Tang, X., Mo, Z., 2021. ZnO nanoparticle-based seed priming modulates early growth and enhances physio-biochemical and metabolic profiles of fragrant rice against cadmium toxicity. Journal of Nanobiotechnology 19(1), 75.

Liaqat, W., Altaf, M.T., Barutçular, C., Mohamed, H.I., Ahmad, H., Jan, M.F., Khan, E.H., 2024. Sorghum: A star crop to combat abiotic stresses, food insecurity, and hunger under a changing climate: A review. Journal of Soil Science and Plant Nutrition 24(1), 74-101.

Mahajan, A., Bhagat, R.M., Gupta, R.D., 2008. Integrated nutrient management in sustainable rice–wheat cropping system for food security in India. SAARC Journal of Agriculture 6(2), 29-32.

Melash, A.A., Bogale, A.A., Bytyqi, B., Nyandi, M.S., Ábrahám, É.B., 2023. Nutrient management as a panacea to improve caryopsis quality and yield potential of durum wheat (*Triticum turgidum* L.) under changing climatic conditions. Frontiers in Plant Science 14, 1232675.

Pandya, P., Kumar, S., Sakure, A.A., Rafaliya, R., Patil, G.B., 2023. Zinc oxide nanopriming elevates wheat drought tolerance by inducing stress-responsive genes and physio-biochemical changes. Current Plant Biology 35, 100292.

Paul, K., Pauk, J., Kondic-Spika, A., Grausgruber, H., Allahverdiyev, T., Sass, L., Vass, I., 2019. Co-occurrence of mild salinity and drought synergistically enhances biomass and grain retardation in wheat. Frontiers in Plant Science 10, 501.

Rao, A., Ahmad, S.D., Sabir, S.M., Awan, S.I., Hameed, A., Abbas, S.R., Ahmad, Z., 2013. Detection of saline tolerant wheat cultivars (*Triticum aestivum* L.) using lipid peroxidation, antioxidant defense system, glycinebetaine and proline contents. Journal of Animal and Plant Sciences 23, 1742-1748.

Raza, M.A.S., Zulfiqar, B., Iqbal, R., Muzamil, M.N., Aslam, M.U., Muhammad, F., Amin, J., Aslam, H.M.U., Ibrahim, M.A., Uzair, M., Habib-ur-Rahman, M., 2023. Morpho-physiological and biochemical response of wheat to various treatments of silicon nanoparticles under drought stress conditions. Scientific Reports 13(1), 2700.

Rehman, S.U., Bilal, M., Rana, R.M., Tahir, M.N., Shah, M.K.N., Ayalew, H., Yan, G., 2016. Cell membrane stability and chlorophyll content variation in wheat (*Triticum aestivum*) genotypes under heat and drought conditions. Crop and Pasture Science 67(7), 712-718.

Sadati, S.Y.R., Godehkahriz, S.J., Ebadi, A., Sedghi, M., 2022. Zinc oxide nanoparticles enhance drought tolerance in wheat via physio-biochemical changes and stress gene expression. Iranian Journal of Biotechnology 20(1), e3027.

Sharma, I., Tyagi, B.S., Singh, G., Venkatesh, K., Gupta, O.P., 2015. Enhancing wheat production: A global perspective. Indian Journal of Agricultural Sciences 85(1), 3-13.

Shewry, P.R., 2009. Wheat. Journal of Experimental Botany 60(6), 1537-1553.

Shiferaw, B., Smale, M., Braun, H.J., Duveiller, E., Reynolds, M., Muricho, G., 2013. Crops that feed the world 10: Past successes and future challenges to the role played by wheat in global food security. Food Security 5(3), 291-317.

Singh, S., Kaur, J., Ram, H., Singh, J., Kaur, S., 2023b. Agronomic bio-fortification of wheat (*Triticum aestivum* L.) to alleviate zinc deficiency in humans. Reviews in Environmental Science and Bio/Technology 22(2), 505-526.

Singh, S.K., Barman, M., Sil, A., Prasad, J.P., Kundu, S., Bahuguna, R.N., 2023a. Nutrient biofortification in wheat: Opportunities and challenges. Cereal Research Communications 51(1), 15-28.

Soleimani, M., Kaghazchi, T., 2007. Agricultural waste conversion to activated carbon by chemical activation with phosphoric acid. Chemical Engineering and Technology 30(5), 649-654.

Szerement, J., Szatanik-Kloc, A., Mokrzycki, J., Mierzwa-Hersztek, M., 2022. Agronomic biofortification with Se, Zn, and Fe: An effective strategy to enhance crop nutritional quality and stress defense-A review. Journal of Soil Science and Plant Nutrition 22(1), 1129-1159.

Ullah, A., Nadeem, F., Nawaz, A., Siddique, K.H., Farooq,

M., 2022. Heat stress effects on reproductive physiology and yield of wheat. Journal of Agronomy and Crop Science 208(1), 1-17.

Ullah, I., Toor, M.D., Basit, A., Mohamed, H.I., Gamal, M., Tanveer, N.A., Shah, S.T., 2023. Nanotechnology: An integrated approach towards agriculture production and environmental stress tolerance in plants. Water, Air, and Soil Pollution 234(11), 666.

Valle-García, J.D., Ali, A., Patra, J.K., Kerry, R.G., Das, G., Fernández-Luqueño, F., 2023. Integration of eco-friendly biological and nanotechnological strategies for better agriculture: A sustainable approach. Agricultural and Environmental Nanotechnology: Novel Technologies and Their Ecological Impact, 647-674.

Vilček, J., Torma, S., 2016. Winter wheat (*Triticum aestivum* L.) growth potential in the Slovak rural landscape. Archives of Agronomy and Soil Science 62(2), 235-245.

Wakeham, P., 2013. The medicinal and pharmacological screening of wheatgrass juice (*Triticum aestivum* L.): An investigation into chlorophyll content and antimicrobial activity. Plymouth Student Scientist 6(2), 20-30.

Waterborg, J.H., 2009. The Lowry method for protein quantitation. Protein Protocols Handbook, 7-10.

Publisher's note: EScience Press remains neutral with regard to jurisdictional claims in published maps and institutional affiliations.

Open Access: This article is licensed under a Creative Commons Attribution 4.0 International License, which permits use, sharing, adaptation, distribution and reproduction in any medium or format, as long as you give appropriate credit to the original author(s) and the source, provide a link to the Creative Commons license and indicate if changes were made. The images or other third-party material in this article are included in the article's Creative Commons license, unless indicated otherwise in a credit line to the material. If material is not included in the article's Creative Commons license and your intended use is not permitted by statutory regulation or exceeds the permitted use, you will need to obtain permission directly from the copyright holder. To view a copy of this license, visit http://creativecommons.org/licenses/by/4.0/.